Available online at www.sciencedirect.com
SCIENCE DIRECT®
International Journal of Thermal Sciences 41 (2002) 1101–1111
International Journal of Thermal Sciences
www.elsevier.com/locate/ijts

Heat and fluid flow resulting from the chimney effect in a symmetrically heated vertical channel with adiabatic extensions

Antonio Auletta, Oronzio Manca *

Dipartimento di Ingegneria Aerospaziale, Seconda Università degli studi di Napoli, Real casa dell'Annunziata, Via Roma 29, 81031 Aversa (CE), Italy

Received 4 May 2001; accepted 7 January 2002

Abstract

An experimental study on a channel-chimney system was carried out in order to elucidate the behavior of heat transfer and fluid flow. The results are presented in terms of local air temperature measurements inside the symmetrically heated channel and between the adiabatic extensions. Different fluid motion regions are observed inside the chimney. Inflows of air are detected in the lower extension ratio, particularly for large values of the ratio of the width of chimney to that of the heated channel. Some typical configurations show the presence of a vortex structure for an expansion ratio greater than one close to the corner regions in the chimney. Some monomial correlation equations between the local Nusselt number, the channel Rayleigh number and the geometric parameters are proposed. The dimensionless parameters are in the following ranges: $10^2 \leqslant Ra^*(B/b) \leqslant 10^6$; $1.5 \leqslant L/L_h \leqslant 4.0$; $1.0 \leqslant B/b \leqslant 4.0$, in which L is the total height of the system, L_h is the height of the heated channel, B is the width of the chimney and b is the width of the heated channel. A good agreement between the correlation and the experimental data is observed.

Keywords: Natural convection; Vertical channel; Experimental analysis; Enhancement of heat transfer; Uniform heat flux; Temperature measurements

1. Introduction

The use of adiabatic extensions downstream of a heat sink or a heated vertical channel enhances natural convective transfer in the heated part of a system [1–6]. Optimal configurations can be obtained for heat sink-chimney systems [1–4] and channel-chimney systems [4,5]. With reference to heated vertical channel-chimney systems, their thermal performance depends on the Elenbaas number (or channel Rayleigh number) as well as two non-dimensional geometric parameters: the extension ratio (total height of the system / height of the channel) and the expansion ratio (chimney spacing / channel spacing).

Several studies have been carried out on the chimney effect both numerically and experimentally [1–3,5–12], as recently reviewed in [6]. The experimental studies are briefly reviewed in the following.

The heat sink-chimney system was studied experimentally in [3,4]. In [3] a vertical parallel-plate finned heat sink with a chimney was investigated. Results obtained using air confirmed to within 11% theoretical predictions of the overall heat transfer and location of optima given in [1]. Flow-field measurements validated momentum transfer and cold inflow at the chimney exit. The measured average chimney velocity was found to be close to that predicted by the theory. Periodic cold inflow at the chimney exit was quantified by its frequency and found to reduce overall heat transfer by approximately 4%. The experiments confirmed that a chimney, when combined with free convection heat sinks resulted in enhanced heat transfer, and therefore permitted the use of smaller geometric dimensions. In [4] the performance a of a pin-fin heat sink with a chimney was obtained. Increased chimney height was shown to reduce the heat-sink temperature by as much as 30%. The experiments were compared with theoretical predictions and reasonable agreement was observed for overall heat transfer, optimal heat-sink porosity and fluid velocity. Finally, the phenomenon of periodic cold inflow at the chimney exit was observed and quantified. Results confirmed the same conclusions obtained in [3].

* Corresponding author.
E-mail addresses: antonio.auletta@unina2.it (A. Auletta), manca@unina.it (O. Manca).

1290-0729/02/$ – see front matter
PII: S1290-0729(02)01396-0

Nomenclature

b	channel spacing ..... m	x, y	coordinates ..... m
B	extension spacing ..... m	x^*, y^*	dimensionless coordinates, Eqs. (1) and (2)
g	acceleration of gravity ..... $m{\cdot}s^{-2}$	*Greek symbols*	
k	thermal conductivity ..... $W{\cdot}m^{-1}{\cdot}K^{-1}$	β	volumetric coefficient of expansion ..... K^{-1}
L	total length, $= L_h + L_{ext}$ ..... m	ν	kinematic viscosity ..... $m^2{\cdot}s^{-1}$
L_{ext}	extension length ..... m	*Subscripts*	
L_h	channel length ..... m	c	convective
Nu_x	local Nusselt number, Eq. (7)	k	conductive
Pr	Prandtl number	max	maximum
q	heat flux ..... $W{\cdot}m^{-2}$	r	radiative
r^2	regression coefficient	ref	reference
Ra_x	local Rayleigh number, Eq. (3)	w	wall
Ra^*	channel Rayleigh number, Eq. (4)	Ω	Ohmic
T	temperature ..... K	0	environmental air
ΔT^*	dimensionless temperature, Eq. (6)		

The channel-chimney system was investigated experimentally in [5–7,11]. In [5] the experiments were performed with air, using a Mach–Zehnder interferometer, providing verification of numerical results for both the local and global changes in heat transfer. The increase in heat transfer rates varied from 2.5 times at low Rayleigh numbers to 1.5 times at high Rayleigh numbers. The authors proposed a single correlation in terms of the channel Rayleigh number and all the geometrical parameters (heated length ratio, expansion ratio). The channel-chimney system with the channel heated was studied experimentally in [6,11] where results were derived in terms of geometric parameters and Rayleigh numbers. The experiments focused for Rayleigh numbers greater than 1.8×10^2 and wall temperature profiles as a function of the extension ratios were presented. Furthermore, the optimal channel configurations were derived, which yielded the minimum value of the maximum wall temperature. Correlations for both dimensionless maximum wall temperature and average channel Nusselt numbers were proposed.

In the case of asymmetrical heating, a cold inflow (downflow) is present, as observed in [3,4] for a heat sink-chimney system, or in [13] for the simple channel and in [7] for a channel-chimney system. Experimental investigations can allow a better understanding of fluid motion inside the chimney as a result of temperature measurements.

It is necessary to have a better understanding of what happens in the chimney in order to improve the heat transfer in the heated part of the system. Experimental investigations of air flow in the chimney provide descriptions of different kinds of motion which take place in the chimney, and local evaluations against which computer codes can be validated. It seems that there is a lack of experimental results on the channel-chimney system with symmetrical heating.

In this paper, an experimental study of a vertical channel-chimney system is carried out. The channel is symmetrically heated with a uniform heat flux. Results in terms of local temperature profiles inside the heated channel and between the insulated walls are presented. Local Nusselt number profiles along the channel height are shown and correlations between local Nusselt and Rayleigh numbers and geometrical dimensionless parameters are proposed.

2. Experimental apparatus

The test section that was investigated is shown schematically in Fig. 1, where x and y are the coordinates in the axial direction and normal to the heated walls, respectively. The channel was made of two symmetrically heated vertical parallel plates, with a length, L_h, equal to 100 mm, and a downstream unheated region (*chimney*), with a length, L_{ext}, that ranged between 0 and 300 mm. The channel and the chimney were 475 mm wide. The channel was made of two heated plates, each of them a phenolic fiberboard 3.2 mm thick and 530 mm wide. The thermal conductivity was 0.17 $W{\cdot}m^{-1}{\cdot}K^{-1}$. The surfaces facing the channel were coated with a 16 μm thick copper layer. The heater on each plate was obtained by cutting the copper layer into a Greek fret. Its copper tracks were 9.6 mm wide, with an approximately 0.5 mm gap between two adjacent tracks, giving the heater a total length of 9.0 m. The expected electric resistance of the circuit was 0.50 Ω. In order to reduce conductive heat losses, a 150 mm polystyrene block was affixed to the rear face of each plate. The chimney was made of two polystyrene plates with a thickness of 30 mm, a width of 530 mm and with a length equal to L_{ext}. The side walls of the channel and chimney were made of plexiglas plates machined to an accuracy of ±0.03 mm. The spacing between the plates was measured to an accuracy of ±0.25 mm by a dial-gauge equipped caliper. The plates were open to the environment along their lower and upper edges. The plates were vertically aligned with horizontal leading edges

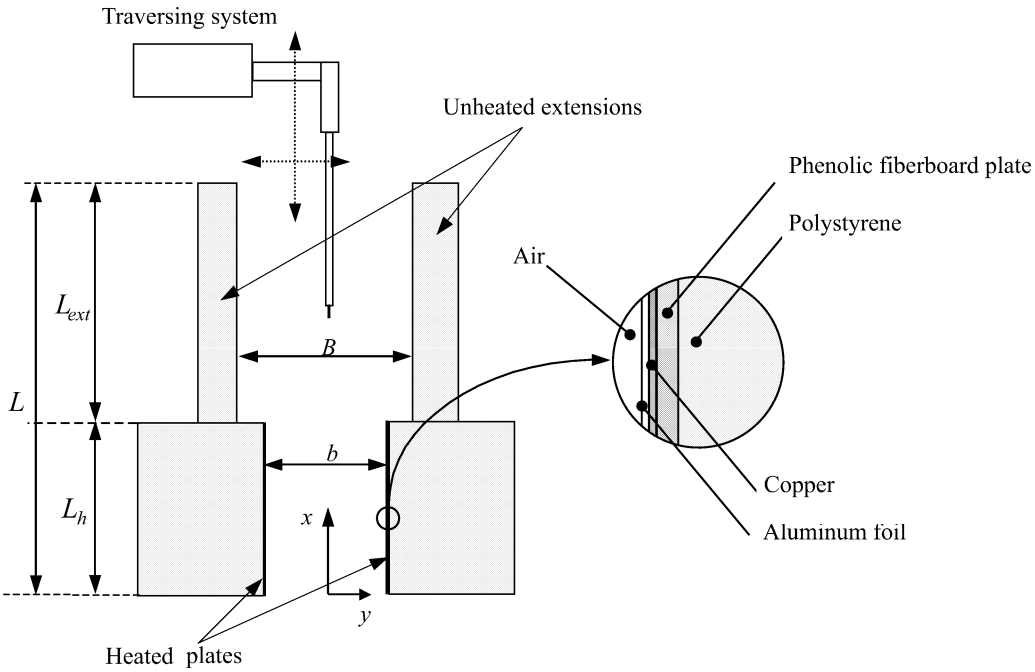

Fig. 1. Sketch of the apparatus.

by screws using a plumb line and a level. The entire apparatus was located in an enclosed room that was carefully sealed in order to eliminate extraneous air currents and air drafts were further reduced by vertical screens, 2.5 m high. In the lower part of the screens were some vents 0.20 m high. The plates were heated by passing a direct electrical current through the copper tracks. This was accomplished by using a Hewlett–Packard E3632A stabilized power supply. The electrical power supplied by each heater was evaluated by measuring the voltage drop across the plates and the current flowing through them. A HP-3465A digital multimeter measured voltage drops in the circuit and across a reference resistance to evaluate the current. To avoid electrical contact resistance, thick copper bars soldered both to the electric supply wire and to the ends of each heater, were bolted together. The dissipated heat flux per board was evaluated with an accuracy of $\pm 2\%$. Wall temperature measurements were carried out by ten equally spaced 0.50 mm OD copper-constantan (type T) thermocouples, embedded and located in the centerline of each plate inside the fiberboard very close to the back side of the copper layer and bonded with a 3 M epoxy glue. They were run horizontally, parallel to the surfaces, thereby lying along isotherms in order to minimize conduction heat losses in the leads. The measured differences in the air ambient temperature in the proximity of the inlet and the exit sections of the apparatus were less than 0.8 K. A further two T-type thermocouples were used to measure the environmental air temperature and the inlet air temperature. A Tersid Isotech Ice Point was used as a reference for the junctions of the thermocouple. A National Instruments SCXI 1000 module data acquisition system and a personal computer were used for the data collection and reduction. The data acquisition was performed by means of LabView^{TM} software. The temperature of the air flowing in the channel and in the chimney was measured using a DANTEC 5600 hot wire system. A 55P15 special miniature probe with a wire of 1 μm diameter and a 56C01–56C20 constant current bridge were used. The probe was calibrated in air, in the temperature range 15–80 °C, by comparison with a T-type thermocouple. The air temperature was measured with a maximum uncertainty of ± 0.1 °C. The probe could be manually positioned anywhere in the channel using a micrometer traversing mechanism supported on the top of the frame (Fig. 1). It allowed positioning of the probe along x and y axes to an accuracy of not less than 0.03 mm. The typical time interval required to attain steady-state conditions after modifying the electric power supply was nearly 3 hours. The probe signal was automatically time averaged by the built-in integrator voltmeter with an integration time of 100 seconds. The air temperature was evaluated on the average of four successive integrated samples.

3. Data reduction

The dimensionless coordinate in the vertical direction is defined by:

$$x^* = x/L_h \tag{1}$$

while the dimensionless coordinate in the horizontal direction is given by:

$$y^* = y/(b/2) \tag{2}$$

The local Rayleigh number is defined as:

$$Ra_x = \frac{g\beta q_c(x)x^4}{\nu^2 k}Pr \tag{3}$$

where $q_c(x)$ is the local convective heat flux, and the channel Rayleigh number is:

$$Ra^* = \frac{g\beta q_c b^5}{\nu^2 k L_h}Pr \tag{4}$$

where q_c is the mean value of the spatially-averaged convective heat flux:

$$q_c = \frac{1}{L_h}\int_0^{L_h} q_c(x)\,\mathrm{d}x \tag{5}$$

The dimensionless air temperature is given by:

$$\Delta T^* = \frac{T - T_0}{qb/k} \tag{6}$$

The local Nusselt number is based on the difference between the wall and the inlet fluid temperatures, rather than on that between the wall and the bulk fluid temperatures, since the latter cannot be easily established in practical applications and the ambient temperature, T_0, is more readily available:

$$Nu_x = \frac{q_c(x)x}{(T_w(x) - T_0)k} \tag{7}$$

The properties of the air were evaluated at the reference temperature: $T_{\mathrm{ref}} = \frac{T_w+T_0}{2}$.

Local convective heat flux, $q_c(x)$, was not uniform because of radiative and conductive losses. Experimental data was reduced by first introducing, in the equations presented above, the local heat flux:

$$q_c(x) = q_\Omega - q_k(x) - q_r(x) \tag{8}$$

where q_Ω was the heat flux due to the Ohmic dissipation, which was assumed to be uniform along the plate; $q_k(x)$ denotes the local conduction heat losses from the plates and $q_r(x)$ represents the local radiative heat flux from the plates. For each run, the terms $q_k(x)$ were calculated by a finite difference numerical procedure, a two-dimensional distribution of the temperature being assumed in the polystyrene. The predicted temperatures in significant configurations of the system were previously compared to those measured by the thermocouples embedded in the polystyrene insulation and the agreement was very good. In fact, the maximum deviation between calculated and measured temperatures referred to the measured temperature rise was ±4%. The $q_r(x)$ terms were calculated for each temperature distribution in the walls and channel spacing by dividing each plate into ten equal size strips along the channel, according to the procedure described by Webb and Hill [14].

In the following, with reference to Fig. 1, the expansion ratio is expressed as B/b and the extension ratio is L_h/L, where $L = L_h + L_{\mathrm{ext}}$. In the experiments the length of the chimney, L_{ext} varied in the range 0–300 mm. The channel spacing, b, varied in the range 10–40 mm; that of the chimney, B, varied in the range 10–200 mm. With these dimensions, the channel aspect ratio was in the 2.5–20 range and the expansion ratio B/b ranged between 1.0 and 8.0.

The uncertainty in the evaluated quantities is determined according to the standard single sample analysis recommended in [15,16]. The uncertainty in the values of the air thermophysical properties can be assumed to be negligible. On the basis of Eqs. (3), (4) and (7) and of the maximum percent uncertainties in the values of Ra^* and Ra_x ranges between 5 and 8 percent while the maximum uncertainty in Nu_x is 4 to 7 percent.

4. Results and discussion

4.1. Temperature profiles

In all the runs the heat flux was equal to 450 $\mathrm{W\cdot m^{-2}}$ and the temperature was referred to the ambient temperature.

In Fig. 2 the temperature profiles of the air in the simple channel ($B/b \to \infty$) with an aspect ratio of $L_h/b = 2.5$ are reported. From the analysis of the figure a regular development of temperature profile is observed. The temperatures at $x^* = 0.50$, near the wall ($y^* \approx 0.80$), exceed the corresponding temperatures at $x^* = 0.95$ because of the edge effects due to the heat conduction in the solid wall, toward the insulated block, and with the ambient together with the radiative losses from the heated surfaces.

In Fig. 3 the temperature profiles of the air in the channel with an extension ratio of $L/L_h = 1.5$ and expansion ratios of $B/b = 1.0$ and $B/b = 3.0$ are shown. The Fig. 3(a) shows that the air temperature at the channel outlet rises with respect to the value in the centerline ($x^* = 0.50$) since the unheated walls of the chimney protect the channel from the edge effects. This is because for $B/b = 1.0$ the unheated extension and the heated wall are coplanar. The edge effects

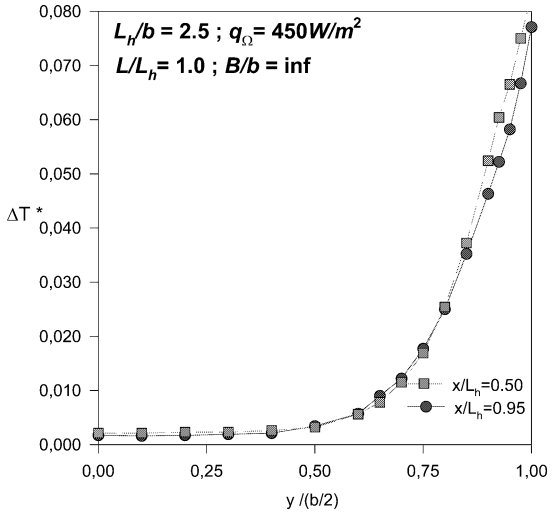

Fig. 2. Temperature profiles for the *base configuration* with $L_h/b = 2.5$.

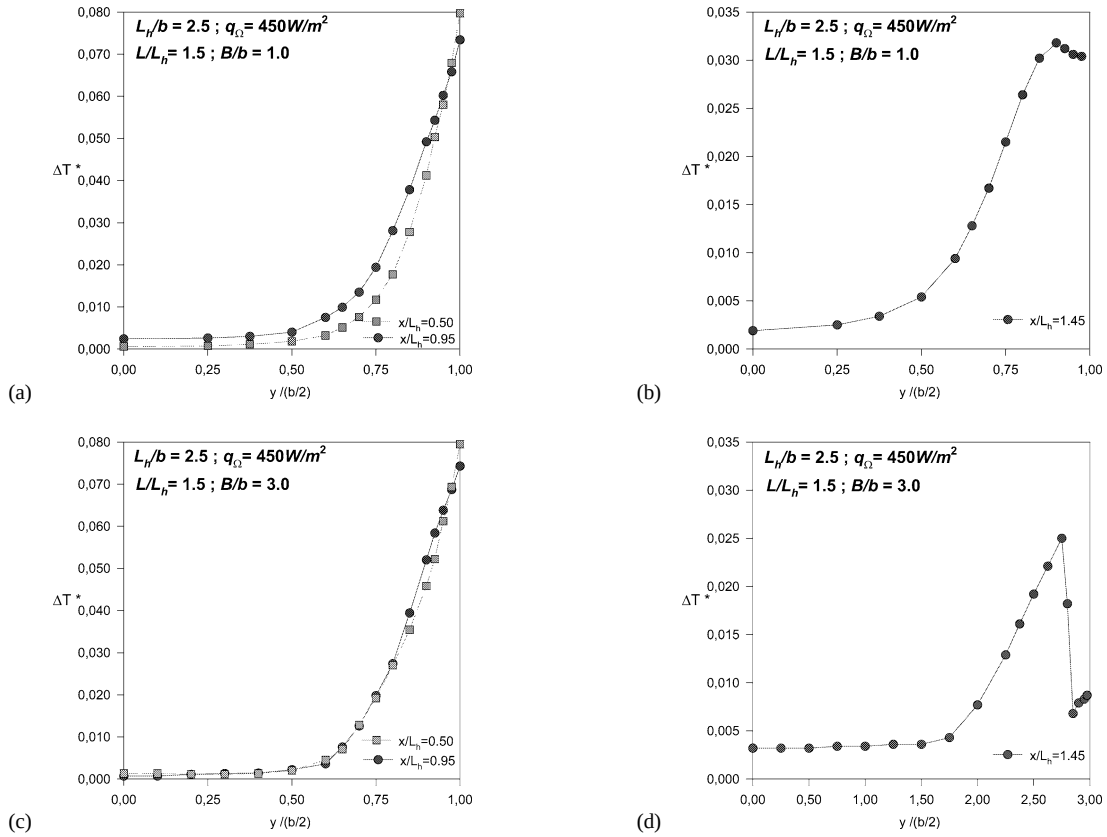

Fig. 3. Temperature profiles for $L/L_h = 1.5$ and $L_h/b = 2.5$: (a) channel, and (b) chimney for $B/b = 1.0$, (c) channel, and (d) chimney for $B/b = 3.0$.

of the heated wall are reduced and the wall temperature, also at the channel outlet, appears higher than in the previous case. The temperature profile near the outlet of the chimney ($x^* = 1.45$) shows an increase up to its maximum value at about $y^* \approx 0.89$, then the temperature decreases due to the heat diffusion toward the colder air ambient close to the outlet of the chimney. In Fig. 3(c) and (d) air temperature profiles in the configuration with an expansion ratio of $B/b = 3.0$ are depicted. In the central zone up to $y^* = 0.75$ the temperature profiles in the channel are similar to those in Fig. 2. A temperature increase is observed at $x^* = 0.95$, where the profile is similar to that shown in Fig. 3(a). Inside the chimney, Fig. 3(d) the bigger expansion ratio than in the previous case results in cooler air close to the insulated wall. The air temperature increases from $y^* \approx 1.75$ up to a maximum value at $y^* \approx 2.75$, followed by a dramatic decrease due to an external inflow. The notable inflow is due to the high expansion ratio ($B/b = 3.0$) and the low extension ratio ($L/L_h = 1.5$). The expanding fluid does not reach the solid wall in the chimney because L_{ext} is small and the depression in the chimney corner is filled by an air inflow from the external environment. This arises because of the inflow of air from the external ambient that laps the chimney wall.

In Fig. 4 the temperature profiles of the air flow for an extension ratio of $L/L_h = 2.0$ and expansion ratios of $B/b = 1.0$ and $B/b = 3.0$ are reported. For $B/b = 1.0$, Fig. 4(a), the temperature profile in the channel is very similar to the case with $L/L_h = 1.0$, and the values are just a little larger than the mean value close to the plate. This is due to the increase of the mass flow rate and, therefore, the heat transfer rate. In the chimney, Fig. 4(b), an increase of temperature can be observed at the mid height of the unheated wall ($x^* = 1.50$) in the central part of the section with respect to the channel outlet profile, that leads the profile to assume a horizontal tangent close to the unheated wall. The temperature profile at the chimney outlet ($x^* = 1.95$) presents more developed values at the centre of the section while, near the wall, the diffusion of heat to the ambient air or the inflow results in the cooling of the air. For an expansion ratio of $B/b = 3.0$, Fig. 4(c) in the channel the temperature profiles are very similar to those of the previous cases and with the curve values relative to $x^* = 0.5$ higher in the region ranging between $y^* = 0.50$ and $y^* = 1.0$. In the chimney (Fig. 4(d)), on the other hand, it can be noted that the profile at mid-height presents a maximum point for $y^* \approx 2.25$ and, in the central zone, higher temperature values are reached than at the outlet. The temperature profile at the outlet of the chimney shows a low average value caused by a probable air inflow both in the central part, due to the expansion in the chimney itself, and near the insulated wall. The air inflow also determines the cooling of the inner region where the heat transfer is more strongly diffusive.

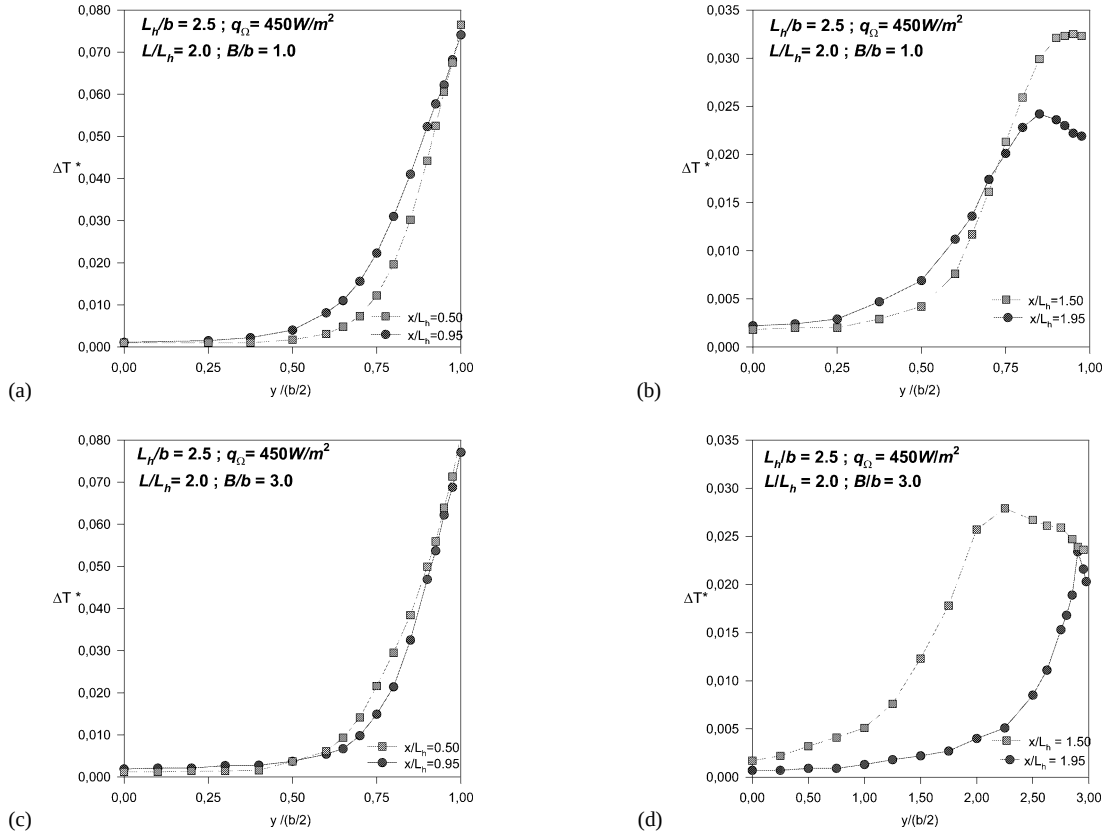

Fig. 4. Temperature profiles for $L/L_h = 2.0$ and $L_h/b = 2.5$: (a) channel and (b) chimney for $B/b = 1.0$, (c) channel, and (d) chimney for $B/b = 3.0$.

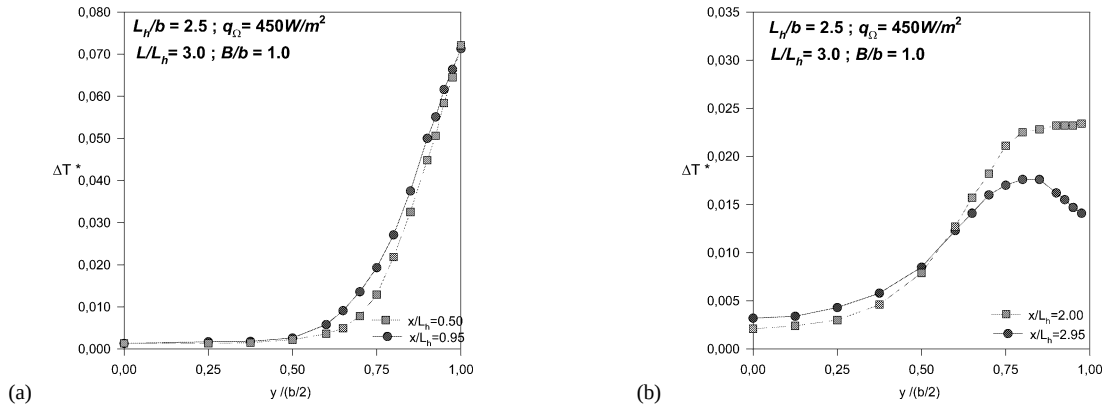

Fig. 5. Temperature profiles for $L/L_h = 3.0$ and $L_h/b = 2.5$: (a) channel, and (b) chimney for $B/b = 1.0$.

The temperature profiles of the air flow in the channel with an expansion ratio of $B/b = 1.0$ and an extension ratio of $L/L_h = 3.0$ are shown in Fig. 5. Inside the channel, profiles very similar to those analyzed in Fig. 4(a) and (c) are noted; some differences are observed only in the zone of the chimney close to the wall where the horizontal region of the temperature profile is reached earlier and the inflow at the outlet determines less temperature values with respect to the previous case.

The temperature profiles in the chimney for the configuration with $B/b = 3.0$ and $L/L_h = 3.0$ are reported in Fig. 6(a). The profile at $x^* = 2.0$ presents minimum values at the center for almost all the width b of the channel, perhaps due to the almost complete expansion of current in the insulated region that determines a depression in the central zone of the chimney. This takes place in such away that, in the same region, there is a cold inflow toward the central zone. The temperature increases up to a maximum value localized around $y^* = 2.25$. The profile shows a relative minimum between the maximum point and the wall. This is, probably, caused by a vortex cell present between the principal current and the insulated wall, as sketched in Fig. 6(b). The probe, starting from the principal current, moving along the y coordinate toward the adiabatic wall meets the ascending branch

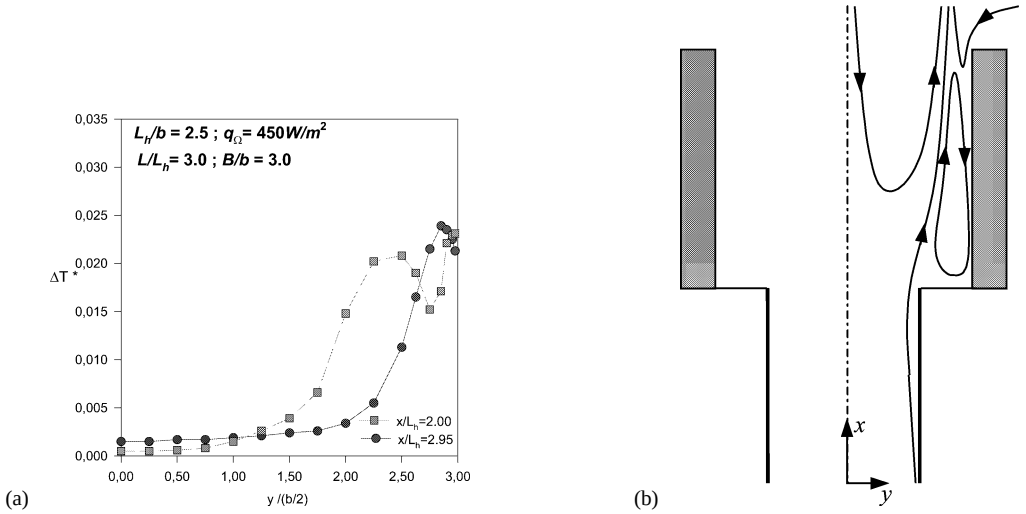

Fig. 6. Temperature profiles for $L/L_h = 3.0$ $L_h/b = 2.5$: (a) chimney, and (b) sketch for $B/b = 1.0$.

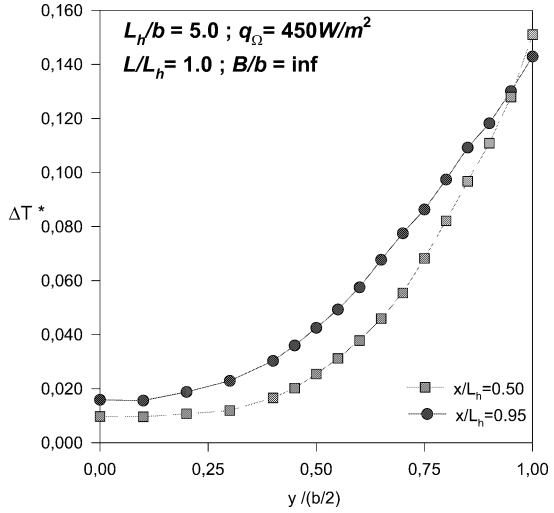

Fig. 7. Temperature profiles for the *base configuration* with $L_h/b = 5.0$.

of the vortex in this region and has a temperature at a value close to that of the principal current. The temperature decreases in the inner region of the vortex. Finally, close to the insulated wall, the probe is surrounded by the descending branch of the vortex. At $x^* = 2.95$ it is noticeable that the temperature profile is practically flat up to $y^* \approx 2$, whereas the probe meets the principal flow. Then, the temperature increases to $y^* = 2.75$ where a weak inflow determines a small lowering as shown in Fig. 6(b).

The base configuration ($B/b \to \infty$) with an aspect ratio of $L_h/b = 5.0$ is shown in Fig. 7. In this case, more developed profiles are observed and, therefore, higher temperature values in the central zone, in contrast to the previous case. An appreciable difference between the profiles at $x^* = 0.50$ and at $x^* = 0.95$ is apparent. This is a consequence of the lower value of Rayleigh number that determines a higher diffusion in the inner layer of the channel. The profile at $x^* = 0.95$ runs almost completely above the profile at $x^* = 0.5$ except near the heated wall where the edge effects invert this path.

Similar behavior is observed in the diagrams in Fig. 8, related to the configurations characterized by an expansion ratio of $B/b = 1.0$ and $B/b = 2.0$ and by an extension ratio of $L/L_h = 2.0$. The temperature profiles of the inner zone are more developed than those relative to the case of $L_h/b = 2.5$ and are similar to those observed in the base case. However, it is noticeable that the profiles in the middle part of the channel and at the exit are always very close to each other, particularly in the case of $B/b = 2$. In Fig. 8(b), however, it is observed how both temperature profiles exhibit an internal maximum point. Furthermore, the temperature values of the air near the exit are almost all less than those relative to $x^* = 1.50$. This could indicate a more efficient heat transfer with the external environment caused by a possible inflow in the chimney outlet. The configuration in Fig. 8(d) shows that the internal layers are hotter than those at the exit of the channel. This is due to the transfer of energy from the layers adjacent to the insulated walls of the chimney. The temperature profiles move slowly with an horizontal tangent toward the wall. At the outlet,in the internal zone, temperatures are higher than those in the previous case and there is a cooling of the air probably caused by a small inflow from outside the channel.

4.2. Local Nusselt numbers and correlations

In Figs. 9 and 10 the profiles of the local Nusselt numbers are portrayed as functions of the dimensionless coordinate x^*, relative to the channel (the heated part of the analyzed system) for some values of heat flux q, and of aspect ratio, L_h/b, expansion ratio, B/b, and extension ratio, L/L_h, investigated. First of all, the growing path of Nu_x should be observed: the presence of the local abscissa in the definition of the Nusselt number clearly conditions this profile. Furthermore, it is noted how, in consonance with geometrical conditions, the profiles are very similar to each

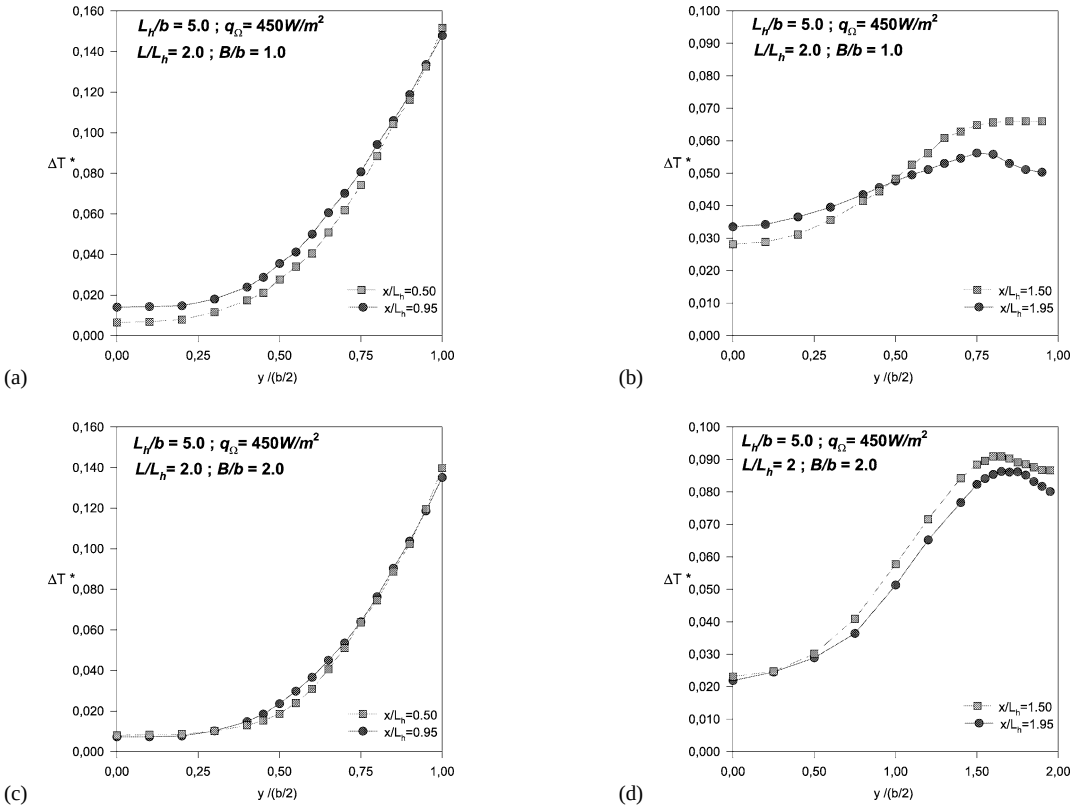

Fig. 8. Temperature profiles for $L/L_h = 2$ and $L_h/b = 5.0$: (a) channel, and (b) chimney for $B/b = 1.0$, (c) channel, and (d) chimney for $B/b = 2.0$.

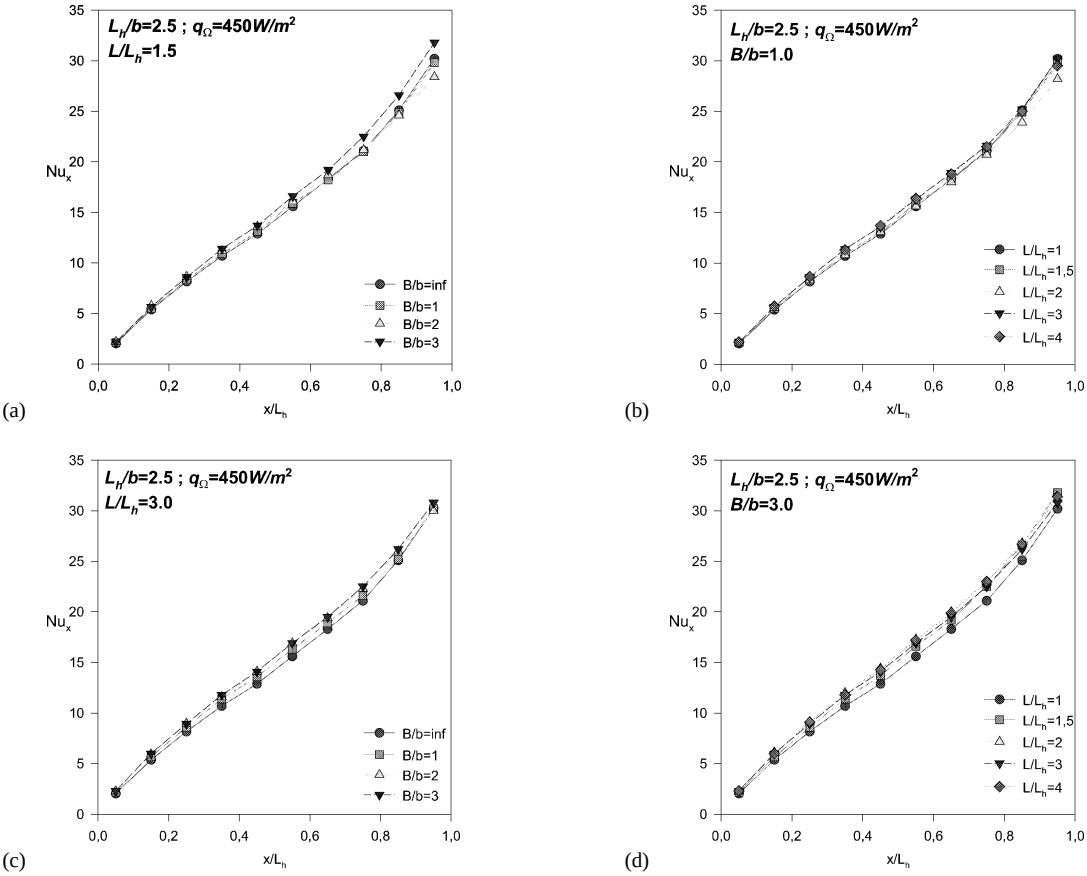

Fig. 9. Local Nusselt number profiles for $L_h/b = 2.5$ and for some values of L/L_h and B/b.

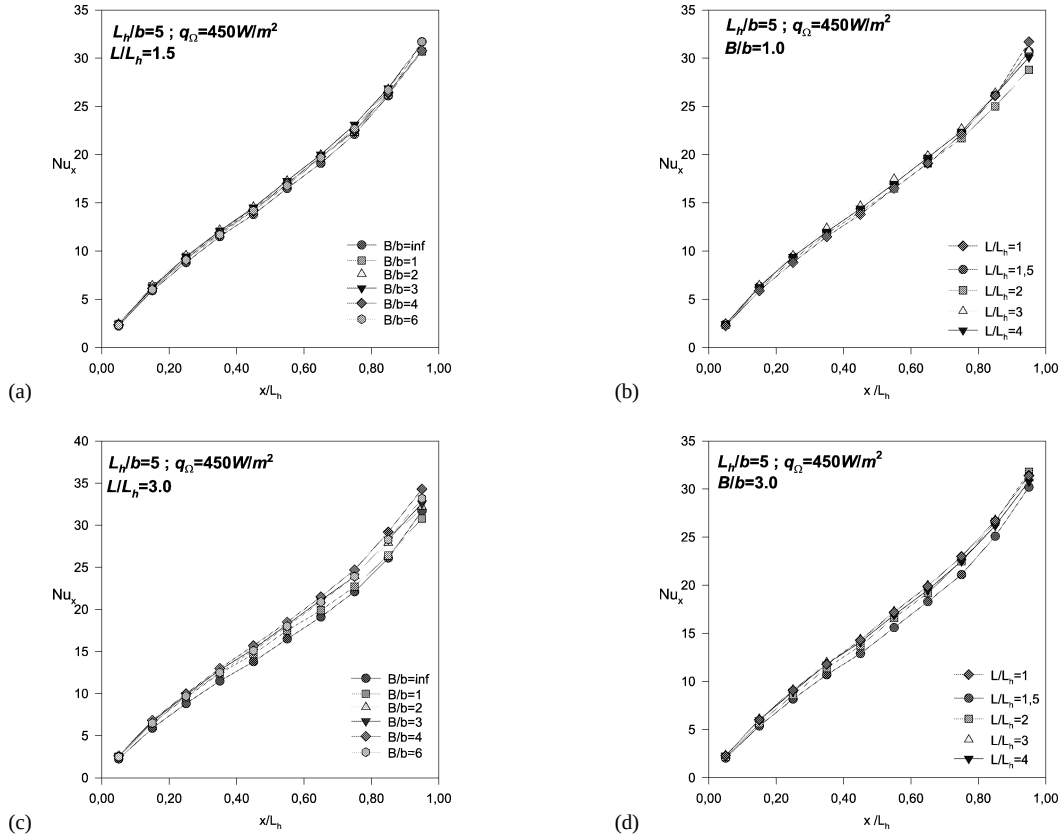

Fig. 10. Local Nusselt number profiles for $L_h/b = 5.0$ and for some values of L/L_h and B/b.

Table 1
Coefficients for Eq. (9)

L/L_h	1.5	2.0	3.0	4.0
a	0.592	0.614	0.618	0.618
b	0.211	0.210	0.210	0.210
c	0.0123	0.0474	0.0556	0.0630
r^2	0.986	0.986	0.988	0.987

other. This demonstrates a weak influence on both B/b and L/L_h for both the aspect ratio values considered. Such a dependency appears somewhat large as L_h/b increases.

A local Nusselt number correlation, for fixed L/L_h value, was found, in the form:

$$Nu_x = a\,Ra_x^b\left(\frac{B}{b}\right)^c \tag{9}$$

The parameters a, b and c, depending on L/L_h ratios, are shown in Table 1 together with the corresponding regression coefficients. This correlations were obtained in the following range: $1.5 \leqslant L/L_h \leqslant 4.0$; $1.0 \leqslant B/b \leqslant 4.0$; $10^2 \leqslant Ra^*(B/b) \leqslant 10^6$. The b values are practically constant whereas a and c depend on the value of L/L_h. The following empirical expressions were obtained:

$$a = -\left[0.209 + 0.247\left(\frac{L}{L_h}\right)^{-6.31}\right] \quad (\text{with } r^2 = 1.000)$$

$$c = 0.0616 - 0.258\left(\frac{L}{L_h}\right)^{-4.09} \quad (\text{with } r^2 = 0.989)$$

By neglecting the dependence of the Nusselt number on the extension ratio L/L_h and considering the average values for a, b and c coefficients ($\bar{a} = -0.214$, $\bar{b} = 0.210$ and $\bar{c} = 0.0446$) it is possible to obtain the following correlation:

$$Nu_x = 0.611\,Ra_x^{0.210}\left(\frac{B}{b}\right)^{0.0446} \tag{10}$$

with $r^2 = 0.989$. A maximum error of 3.17% occurs for the computation of a and an error of 2.52% for the computation of $(B/b)^c$ using $\bar{a}$ and $\bar{c}$ instead of $a(L/L_h)$ and $c(L/L_h)$.

For a channel without extensions (*base configuration*) the following correlation was found:

$$Nu_x = 0.556\,Ra_x^{0.215} \tag{11}$$

with $r^2 = 0.987$. By fixing, instead, the exponent of Rayleigh number at 1/5, the following result is obtained:

$$Nu_x = 0.675\,Ra_x^{0.20} \tag{12}$$

with $r^2 = 0.983$; this result is in very good agreement with the classical results for the simple channel [17–19]. A correlation in terms of local Nusselt number at channel midheight, $Nu_b(L_h/2)$, and channel Rayleigh number, Ra^*, is carried out to obtain a comparison between the present data and the correlation equations given in [17–19]. The $Nu_b(L_h/2)$ is defined as:

$$Nu_b(L_h/2) = \frac{q_c(L_h/2)}{(T_w(L_h/2) - T_0)}\frac{b}{k} \tag{13}$$

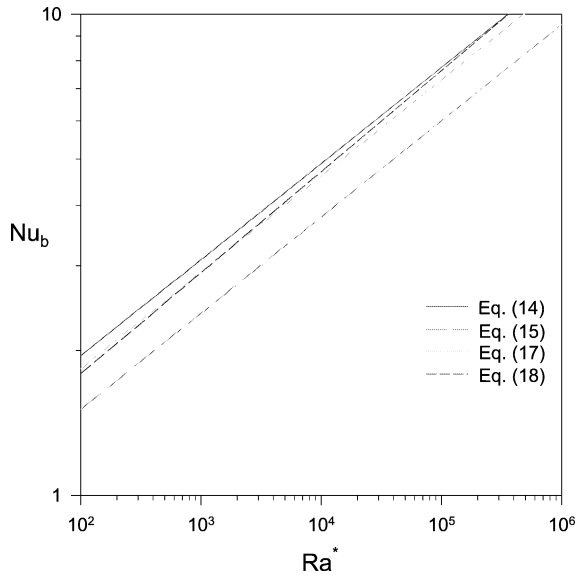

Fig. 11. Comparison between correlation equations of Nusselt and Rayleigh numbers obtained by present data, Eq. (14), and existing literature: in [17] Eq. (15), in [18] Eq. (17) and in [19] Eq. (18).

and by Eq. (12) is obtained:

$$Nu_b(L_h/2) = 0.775\,Ra^{*0.20} \tag{14}$$

The following equation is given in [17]:

$$Nu_b(L_h/2) = 0.60\,Ra^{*0.20} \tag{15}$$

The correlation equations given in [18,19] are given in terms of the average Nusselt number Nu_b defined as

$$Nu_b = \frac{q_c}{(T_w - T_0)}\frac{b}{k} \tag{16}$$

where $(T_w - T_0)$ is the average wall temperature rise. The equations for Nu_b are:

$$Nu_b = 0.73\,Ra^{*0.20} \tag{17}$$

given in [18] and

$$Nu_b = 0.68\,Ra^{*0.21} \tag{18}$$

given in [19]. In Fig. (11) Eqs. (14), (15) and (17), (18) are compared. It is noted that the agreement between Eq. (14) and Eqs. (17) and (18) is very good whereas a slight difference is observed with Eq. (15).

5. Conclusions

An experimental investigation of a symmetrically heated vertical channel with adiabatic extensions downstream (chimney) has been presented in terms of local air temperature measurements. Temperature profiles in a heated channel and between insulated extensions were obtained to show the effects of the geometric parameters on the buoyancy driven in the heated channel and in the chimney. It was found that the dependence of heat transfer in the heated channels is affected only weakly by the adiabatic extensions.

Different regions of fluid motions were detected inside the chimney, particularly when the expansion ratio was greater than one. In fact, in this case, an abrupt expansion of the air, a vortex structure close to the corner zone and a downflow motion were shown. At the same B/b value, the larger the extension ratio L/L_h the lesser the temperature decrease close to the adiabatic wall in the chimney outlet region. On the other hand, for fixed L/L_h, the bigger expansion ratio B/b the greater the downflow in the chimney, while the central cooler region in the chimney is more expanded.

Local Nusselt number profiles appeared to be weakly influenced by the geometric parameters. However, for higher value of L_h/b (=5) this dependence appeared slightly greater.

Some correlation equations between the local Nusselt number, the channel Rayleigh number, the expansion ratio and the extension ratio were proposed. The correlations were monomial in terms of Rayleigh number and the expansion ratio with coefficients depending on the extension ratio. The ranges of the parameters were: $10^2 \leqslant Ra^*(B/b) \leqslant 10^6$; $1.5 \leqslant L/L_h \leqslant 4.0$; $1.0 \leqslant B/b \leqslant 4.0$. The equations were in very good agreement with the experimental results. Moreover, a correlation for the simple channel was also proposed and it was found to be in good agreement with classical results.

Acknowledgements

This research is supported by MURST under 1999 grant research program "*Enhancement Techniques in Thermofluids*". A special acknowledgement is given to the reviewers, their suggestions and comments have improved the article.

References

[1] T.S. Fisher, K.E. Torrance, K.K. Sikka, Analysis and optimization of a natural draft heat sink system, IEEE Trans. Compon. Pack. A 20 (1997) 111–119.
[2] T.S. Fisher, K.E. Torrance, Free convection limits for pin-fin cooling, J. Heat Trans.-T ASME 120 (1999) 633–640.
[3] T.S. Fisher, K.E. Torrance, Experiments on chimney-enhanced free convection, J. Heat Trans.-T ASME 121 (1999) 603–608.
[4] W.W. Thrasher, T.S. Fisher, K.E. Torrance, Experiments on chimney-enhanced free convection from pin-fin heat sinks, J. Electron. Pack. 122 (2000) 350–355.
[5] A.G. Straatman, J.D. Tarasuk, J.M. Floryan, Heat transfer enhancement from a vertical, isothermal channel generated by the chimney effect, J. Heat Trans.-T ASME 115 (1993) 395–402.
[6] A. Auletta, O. Manca, B. Morrone, V. Naso, Heat transfer enhancement by chimney effect in a vertical isoflux channel, Internat. J. Heat Mass Transfer 44 (2001) 4345–4357.
[7] O. Manca, M. Musto, V. Naso, Experimental analysis of chimney effect in a vertical isoflux channel, in: Proceedings of 5th World Conference on Experimental Heat Transfer, Fluid Mechanics and Thermodynamics, Thessaloniki, Greece, 2001, pp. 645–650.

[8] Y. Asako, H. Nakamura, M. Faghri, Natural convection in a vertical heated tube attached to thermally insulated chimney of a different diameter, J. Heat Trans.-T ASME 112 (1990) 790–793.
[9] K.T. Lee, Natural convection in vertical parallel plates with an unheated entry or unheated exit, Numer. Heat Trans. A Appl. 25 (1994) 477–493.
[10] A. Campo, O. Manca, B. Morrone, Numerical analysis of partially heated vertical parallel plates in natural convective cooling, Numer. Heat Trans. A Appl. 36 (1999) 129–151.
[11] N. Bianco, O. Manca, B. Morrone, V. Naso, Experimental analysis of chimney effect for vertical isoflux symmetrically heated parallel plates, in: Proceedings of Thermal Management of Electronic Systems III (Eurotherm Seminar ’58), 1998, pp. 73–79.
[12] G.A. Shahin, J.M. Floryan, Heat transfer enhancement generated by the chimney effect in systems of vertical channel, J. Heat Trans.-T ASME 121 (1999) 230–232.
[13] E.M. Sparrow, G.M. Chrysler, L.F. Azedevo, Observed flow reversal and measured-predicted Nusselt number convection in a one-sided heated vertical channel, J. Heat Trans.-T ASME 106 (1984) 325–332.
[14] G.A. Webb, D.P. Hill, Rayleigh number laminar natural convection in an asymmetrical heated vertical channel, J. Heat Trans.-T ASME 111 (1989) 649–656.
[15] S.G. Kline, F.A. McClintock, Describing uncertainty in single sample experiments, Mech. Engrg. 75 (1958) 3–12.
[16] R.J. Moffat, Describing the uncertainties in experimental results, Exp. Therm. Fluid Sci. 1 (1998) 3–17.
[17] W. Aung, L.S. Fletcher, V. Sernas, Developing laminar free convection between vertical flat plates with asymmetric heating, Internat. J. Heat Mass Transfer. 15 (1972) 2293–2308.
[18] A. Bar-Cohen, W.W. Rosenow, Thermally optimum spacing of vertical, natural convection cooled, parallel plates, J. Heat Trans.-T ASME 106 (1984) 116–123.
[19] O. Manca, S. Nardini, Composite correlations for air natural convection in tilted channels, Heat Transfer Engrg. 20 (1999) 64–70.